energies

MDPI

Article

Reduced Model and Comparative Analysis of the Thermal Performance of Indirect Solar Dryer with and without PCM

Camilo Ramirez [1], Mario Palacio [2] and Mauricio Carmona [1,*]

[1] Rational Use of Energy and Environment Preservation Research Group, Universidad del Norte, Barranquilla 081007, Atlántico, Colombia; arcamilo@uninorte.edu.co

[2] Processes Optimization Rational Energy Use and Biomass Research Group, Universidad Pontificia Bolivariana, Montería 230003, Córdoba, Colombia; mario.palaciov@upb.edu.co

* Correspondence: mycarmona@uninorte.edu.co

Received: 30 July 2020; Accepted: 10 October 2020; Published: 21 October 2020

Abstract: A thermal model is proposed to analyze the performance of an indirect solar dryer (ISD) with latent heat storage using phase change material (PCM). The estimations are compared with experimental data presented in the scientific literature taken in real conditions. The validated thermal model is used in order to address a comprehensive analysis of the performance of the ISDs under the same operation conditions, the model is able to estimate the temperatures of glass cover, absorber plate, PCM, useful heat, thermal and storage efficiencies, and variables that are difficult to measure experimentally such as liquid fraction, heat losses, and accumulated energy of the ISDs. Three study cases are considered: Case 1 consists of two collectors with and without alternating nocturnal and diurnal operation (benchmarking case). Case 2 and 3 consist in a unique collector operating continuously for 24 h with PCM and without PCM, respectively. It was determined that the use of PCM in ISD increased the night thermal performance and extended the operational time of the system. On the other hand, results indicate that the use of two alternating collectors presents similar discharge behavior to using one collector with PCM operating continuously. Concerning the overall thermal performance, cases 1, 2, and 3 obtained thermal efficiencies of 20%, 28%, and 24%, respectively.

Keywords: PCM; thermal model; solar drying; FPSC

1. Introduction

The use of solar radiation for drying processes is a renewable and non-polluting source of energy with the potential to substitute for conventional fossils fuels [1]. The traditional method for solar drying is known as open sun drying. However, it has several disadvantages related to the quality of the product to be dried due to exposure to environmental conditions (rain, dirt, insects, etc.). Different types of solar dryers have been developed over the years to mitigate the disadvantages of open sun drying. These devices improve the drying quality and significantly increase air drying capacity [2]. Solar dryers are classified into indirect, direct, and mixed solar dryers. Direct solar dryers are translucent enclosures that use the greenhouse effect to increase the air temperature and dry the products inside it. Indirect solar dryers consist of a solar air heater and a drying chamber. The moisture content of the product is removed due to contact with air from the solar air heater. The most used solar air heaters in indirect solar drying are flat plate solar collectors [3]. Mixed solar dryers are a combination of the two previous technologies. The solar dryer consists of a solar air heater and a translucent cabin. The pre-heated air enters the cabin, removing the humidity of the product in combination with the greenhouse effect generated in the enclosure [4]. The most used combination for mixed solar dryers is the cabin type and the flat plate solar air heaters [5].

Different authors have investigated to overcome the interruption of the drying process due to the absence of incident solar radiation produced at night or the intermittence due to natural variations in solar energy. One of the most studied approaches to solving this disadvantage is thermal energy storage. In this method, the energy is stored during daylight and then is released at night. Research works commonly classified thermal energy storage for solar dryers into sensible and latent heat [6]. Sensible heat storage is proportional to the specific heat, temperature, and mass accumulation material. This direct relationship with the mass of the material represents an important issue due to the large size required by the storage systems, mainly if the storage material is the same working fluid [7]. In contrast, in latent heat storage, thermal energy is stored/released by material during a phase change process at constant temperature (or in a narrow temperature range) [8]. Regarding phase change materials (PCMs), there are many studies in terms of encapsulation forms [9,10], modeling, applications, and characterizations of PCMs [11–13].

Numerical simulations in solar dryers with thermal energy storage using PCM have been an important research topic. Simulations by numerical models allow the prediction of the thermal behavior of PCMs as storage systems and the estimation of equipment operation parameters. Reyes et al. present a two-dimensional model of a solar air heater with thermal storage in aluminum cans located above the absorber plate. Results show that the model predicts the experimental data with a maximum temperature difference of 7 °C for low airflows [14]. Tchaya et al. concluded that the contact resistance between the absorber plate and thermal storage or thermal insulation should be considered for optimum performance of models for flat plate solar air heaters [15]. A diffusion approximation model was validated for the kinetics of apple drying in an indirect solar dryer with and without PCM as an external thermal energy storage unit [16]. Results show that the model correctly fits the experimental data for the dryer with and without thermal energy storage. Vasquez et al. validated a numeric model for a solar dryer system with two flat plate collectors with and without PCM. Results showed that the one-dimensional model is independent of the number of finite volumes from 30 nodes. The model was validated with experimental data for different air flows and different local conditions [17].

In order to model a solar dryer with PCM, it is necessary to evaluate numerous days of operation due to the nature of solar energy and the environmental conditions in which the equipment is located. Consequently, the solar dryers must be evaluated under dynamic operating conditions with high variability (such as reduction in incident radiation due to high cloudiness or changes in wind speed). This results in very long simulation times and high computational cost. To overcome this issue, zero-dimensional models or reduced models have been implemented over the past years. These models present a new research topic due to their low computational cost and versatility in evaluating different operating scenarios. Most of the current reduced models are implemented for flat plate solar collectors. In solar collectors for water heating, a model was developed for a flat plate solar collector with thermal storage [18]. However, it was not validated with experimental data or scientific research. A reduced thermal model for a flat plate solar collector with latent heat storage was presented by Carmona et al. [19]. Their model was used to identify significant influencing variables in the process. This work compared the results obtained with the traditional collector reported by Dagdougui et al. [20]. In [21], a reduced model for a flat plate solar collector with thermal storage using PCM was presented. The model was validated with experimental data and allows the prediction of the temperatures of the components; it also allows the estimation of parameters that would be difficult to obtain experimentally. In their studies of solar air heaters for solar dryers, Potdukhe et al. presented a reduced thermal model of an indirect solar dryer with sensible heat thermal storage. The model was experimentally validated for different agricultural products and different operating conditions [22]. In [23], a thermal prediction model of a finned solar collector for air heating without thermal energy storage was reported. Simo-Tagne et al. modeled the drying curve in an indirect solar dryer for industrial wood drying. The model was validated with experimental data for different operating conditions of the dryer [24]. A dynamic prediction model for air heating in an indirect solar dryer with a double-pass parallel flow solar collector without energy storage was validated by [25].

Literature review shows no report of a reduced model that estimates the interaction between the main components, charge and discharge cycles, liquid fraction of the PCM, and thermal behavior of solar dryers with thermal energy storage using PCM. In the present paper, a reduced model is presented to analyze the performance of an indirect solar dryer with and without thermal energy storage using PCM. The model was implemented and simulated in MATLAB/Simulink software and was validated with the results reported in 2017 by El Khadraoui et al. [26]. Output variables proposed in their investigation, such as the temperature of the drying chamber with PCM, the heat absorbed by the solar collector, and the heat stored by the PCM were compared. In addition, the effects of conduction, radiation, internal and external convection, energy losses, temperatures of the components, and the solid–liquid phase change of the PCM are estimated by the model under variable operating conditions and compared for three different case studies.

2. Thermal Model

2.1. Assumptions

The model is based on the following assumptions:

- The model invokes the quasi-equilibrium condition for the non-stationary state.
- Heat transfer is considered one-dimensional, and the collector main parts are considered as lumped systems.
- Heat losses through the collector walls are negligible compared with other terms in the energy equation.
- The melting process is considered mainly by conduction due to heating from the top to the bottom.

2.2. Model

The model is based on the energy balance for each component of the flat plate collector: glass cover, work fluid, absorber plate, and PCM container. Figure 1 shows the heat transfer modes involved in the model.

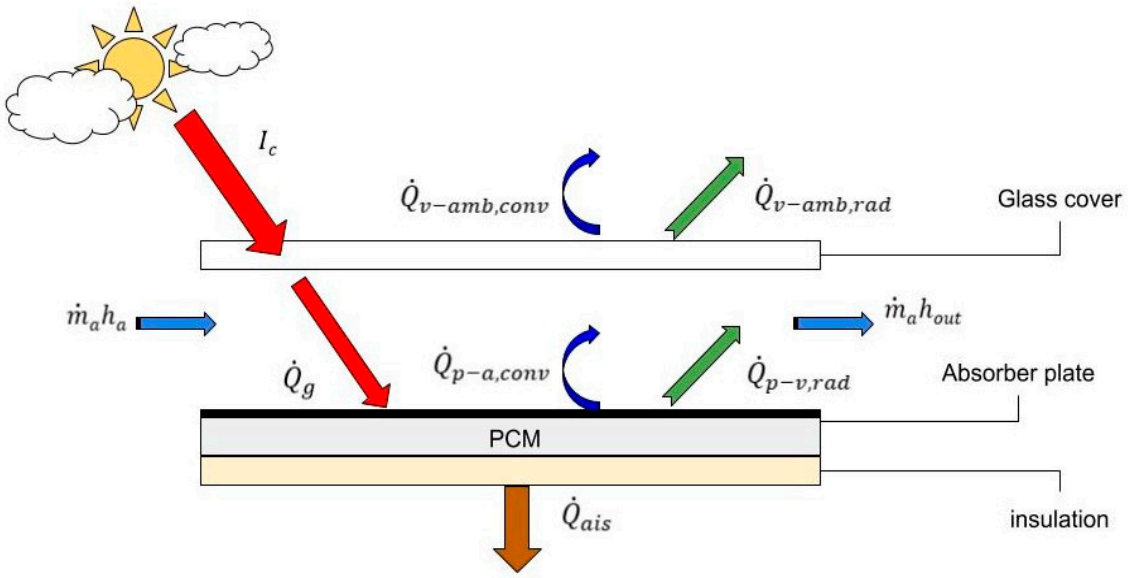

Figure 1. Heat transfer terms involved in the model.

The energy balance in the glass cover is given by

$$\dot{Q}_{p-v,rad} + \dot{Q}_{a-v,\ conv} + \dot{Q}_s - \dot{Q}_{v-amb,rad} - \dot{Q}_{v-amb,conv} = m_v C_{p,v} \frac{\Delta T_v}{\Delta t} \quad (1)$$

where

$$\dot{Q}_s = \alpha_v A_C I_c \tag{2}$$

$$\dot{Q}_{v-amb,rad} = h_{v-amb,rad} A_C (T_v - T_{amb}) \tag{3}$$

$$\dot{Q}_{v-amb,conv} = h_{v-amb,conv} A_C (T_v - T_{amb}) \tag{4}$$

$$\dot{Q}_{p-v,rad} = h_{p-v,rad} A_C \left(T_{pa} - T_v\right) \tag{5}$$

$$\dot{Q}_{a-v,conv} = h_{a-v,conv} A_C (T_a - T_v) \tag{6}$$

where α_v, A_C, I_c, T_{pa}, T_v, T_a, and T_{amb} are the glass cover absorptance, collection area, solar irradiation, absorber plate, cover, mean air, and ambient temperature, respectively. The heat transfer coefficients are given by [27,28]:

The radiation and convection heat transfer coefficients between the top of the cover and the air are given by [29]

$$h_{v-amb,rad} = \sigma \varepsilon_v \left(T_{sky}^2 + T_v^2\right)\left(T_{sky} + T_v\right) \tag{7}$$

$$h_{v-amb,conv} = 5.7 + 3.8 V_{amb} \tag{8}$$

where

$$T_{sky} = 0.0552 T_{amb}^{1.5} \tag{9}$$

σ is the Stefan–Boltzmann constant, ε_v is the cover emissivity, and V_{amb} is the wind velocity.

The radiation heat transfer coefficient between the absorber and glass cover are given by [29]

$$h_{p-v,rad} = \frac{\sigma\left(T_{pa}^2 + T_v^2\right)\left(T_{pa} + T_v\right)}{\frac{1}{\varepsilon_{pa}} + \frac{1}{\varepsilon_v} - 1} \tag{10}$$

The convection heat transfer coefficient between the glass cover and air can be calculated by the Nusselt number given by [28]

$$N_{u,a-v} = 4.9 + \frac{0.0606\left(ReP_r \frac{D_H}{L_{co}}\right)}{1 + 0.0909 P_r^{0.17}\left(ReP_r \frac{D_H}{L_{co}}\right)^{0.7}} \tag{11}$$

$$h_{a-v,conv} = \frac{N_{u,a-v} k}{D_{H1}} \tag{12}$$

where Reynold number Re and hydraulic diameter D_H are defined by these equations:

$$Re = \frac{\rho V D_H}{v} \tag{13}$$

$$D_H = \frac{2 W_{co} H_{co}}{W_{co} + H_{co}} \tag{14}$$

The energy balance in the work fluid is

$$\dot{Q}_{p-a,conv} - \dot{Q}_{a-v,conv} - \dot{Q}_U = m_a C_{p,a} \frac{\Delta T_a}{\Delta t} \tag{15}$$

where

$$\dot{Q}_{p-a,conv} = h_{pa-a,conv} A_C \left(T_{pa} - T_a\right) \tag{16}$$

$$\dot{Q}_U = \dot{m}_a C_{p,a} (T_{out} - T_{amb}) \tag{17}$$

T_{out} and $\dot{m}_a$ are the outlet air temperature and mass flow rate, respectively. The convection heat transfer coefficient between the absorber and air can be calculated with Equations (11)–(14).

The outlet and mean air temperature are related by

$$T_a = \frac{T_{out} + T_{amb}}{2} \tag{18}$$

The energy balance in the absorber plate is

$$\dot{Q}_g - \dot{Q}_{p-v,rad} - \dot{Q}_{p-a,conv} - \dot{Q}_{PCM.u} = m_p C_{p,p} \frac{\Delta T_p}{\Delta t} \tag{19}$$

where $\dot{Q}_g$ and $\dot{Q}_{PCM.u}$ are the absorbed solar radiation and the charge or discharge heat transfer of the PCM. The absorbed solar radiation is given by the equation

$$\dot{Q}_g = \left(\alpha_p \tau_v\right) A_C I_c \tag{20}$$

where α_p, τ_v are absorber plate absorptance and glass cover transmissivity, respectively. The heat transfer of the absorber toward the PCM (in charge) or from the PCM toward the absorber (in discharge) are given by

$$\dot{Q}_{PCM.u} = h_{PCM} A_{PCM} \left(T_p - T_{PCM}\right) \tag{21}$$

where h_{PCM} is the thermal contact conductance related to the absorber plate and the upper layer of the PCM.

The energy balance in the PCM container is given by

$$\dot{Q}_{PCM.u} - \dot{Q}_{PCM.L} = \dot{E}_{PCM.T} \tag{22}$$

The PCM is discretized in order to model the heat transfer through it. The PCM is divided into n_{PCM} layers, and an energy balance is generated in each layer. The energy balance for the first layer (the upper layer) is given by [21]

$$\dot{Q}_{PCM.u} - \dot{Q}_{PCM\ 1:2} = \dot{E}_{PCM.1} \tag{23}$$

The energy balance for an intermediate layer (i) can be calculated by

$$\dot{Q}_{PCM\ i-1:i} - \dot{Q}_{PCM\ i:i+1} = \dot{E}_{PCM.i}. \tag{24}$$

where $\dot{Q}_{PCM\ i-1:i}$ is the heat transfer from a superior layer, and $\dot{Q}_{PCM\ i:i+1}$ is the heat transferred to the lower layer. The energy balance for the last layer (n) is calculated by

$$\dot{Q}_{PCM\ n-1:n} - \dot{Q}_{PCM\ L} = \dot{E}_{PCM.n} \tag{25}$$

where $\dot{Q}_{PCM\ L}$ is the heat transfer from the PCM to the ambient air (through insulation), and it is given by

$$\dot{Q}_{PCM\ L} = h_{los} A_{PCM} (T_{PCM.n} - T_{amb}) \tag{26}$$

where h_{los} is the conductance through the insulation.

$$h_{los} = \frac{k_{ins}}{L_{ins}} \tag{27}$$

The energy is stored in each layer in terms of sensible and latent heat, and it is represented by the equation

$$\dot{E}_{PCM.i} = \dot{E}_{PCM\ sensible.i} + \dot{E}_{PCM\ latent.i} \tag{28}$$

where

$$\dot{E}_{PCM\ sensible.i} = m_{PCM.i} C_{p\ solid} \frac{\Delta T_{PCM.i}}{\Delta t} \tag{29}$$

$$\dot{E}_{PCM\ latent.i} = m_{PCM.i} h_{fg} \frac{\Delta \lambda_{PCM.i}}{\Delta t} \tag{30}$$

where $\lambda_{PCM.i}$ is the liquid fraction of the layer i. The liquid fraction is calculated in each PCM layer when the temperature of the layer is equal to the melting point of the material, in that case the accumulated energy in each layer is divided by the PCM's latent heat of fusion. The total liquid fraction is obtained by dividing the sum of the liquid mass of all layers by the total mas of the PCM as presented in the following equation.

$$\lambda_i = \frac{m_{PCM\ liquid.i}}{m_{PCM.i}} = \frac{m_{PCM.i} - m_{PCM\ solid.i}}{m_{PCM.i}} \tag{31}$$

The total energy stored in the PCM is given by

$$\dot{E}_{PCM.T} = \sum_{i=1}^{n_{PCM}} \dot{E}_{PCM.i} \tag{32}$$

If the temperature of the PCM is different from the phase change temperature ($T_{PCM.i} \neq T_M$), the latent heat term $\dot{E}_{PCM\ latent.i}$ is equal to 0, in this case $\frac{\Delta \lambda_{PCM.i}}{\Delta t} = 0$.

In the other case, if the temperature of the PCM is equal to the phase change temperature ($T_{PCM.i} = T_M$), the sensible heat term $\dot{E}_{PCM\ sensible.i}$ is equal to 0, for this case $\frac{\Delta T_{PCM.i}}{\Delta t} = 0$.

Finally, the thermal and storage accumulated efficiency can be calculated as

$$\eta_{th} = \frac{\int_a^b \dot{Q}_U dt}{\int_a^b A_C I_c dt} \tag{33}$$

$$\eta_{std} = \frac{\int_a^b \dot{Q}_{U.dis} dt}{\int_a^b A_C I_c dt} \tag{34}$$

2.3. Model Inputs and Outputs

The input variables of the model consist of the outdoor operating conditions and are shown in Table 1. These variables are entered into the model dynamically.

Table 1. Input variables.

Variable	Notation	Units
Ambient temperature	T_{amb}	°C
Solar radiation	$\dot{q}_s$	w/m^2
Wind velocity	V_{amb}	m/s
Mass air flow rate	$\dot{m}_a$	kg/s

The input parameters are shown in Table 2 and correspond to the dimensions, characteristics, and properties of the multiple components of the ISD.

Table 2. Input parameters.

Component	Parameter	Value	Units
Glass cover	Specific heat	834	J/kg·K
	Density	2700	kg/m^3
	Emissivity	0.94	-
	Absorptivity	0.05	-
	Transmissivity	0.81	-
	Dimension	$2.04 \times 1.04 \times 0.004$	m
Absorber plate	Specific heat	390	J/kg·K
	Density	8960	kg/m^3
	Emissivity	0.9	-
	Absorptivity	0.9	-
	Dimension	$2.04 \times 1.04 \times 0.001$	m
PCM	Melting temperature	56–60	°C
	Heat of fusion	214,400	kJ/kg
	Density	775	kg/m^3
	Thermal conductivity	0.21	W/m·K
	Dimension	$2.04 \times 1.04 \times 0.06$	m
Insulation	Thermal conductivity	0.028	W/m·K
	Thickness	0.05	m

The model predicts the thermal behavior of the ISD, providing as response variables the temperature of the main components, the heat fluxes, the energy accumulated in components, the liquid fraction of the PCM, the thermal, and storage efficiency of the device. All the response variables of the model are dynamically calculated and are presented in Table 3.

Table 3. Output variables.

Variable	Notation	Units
Glass cover temperature	T_v	°C
Absorber plate temperature	T_{pa1}	°C
PCM temperature	T_{PCM}	°C
Useful heat rate	$\dot{Q}_U$	W
Radiation loss	$\dot{Q}_{v-amb,rad}$	W
Convection loss	$\dot{Q}_{v-amb,conv}$	W
Insulation loss	$\dot{Q}_{PCM.L}$	W
Total losses heat rate	$\dot{Q}_{loss}$	W
Stored heat rate	$\dot{Q}_{PCM}$	W
Glass cover accumulated energy	$\dot{E}_v$	Wh
Absorber plate accumulated energy	$\dot{E}_{pa1}$	Wh
PCM accumulated energy	$\dot{E}_{PCM}$	Wh
Total accumulated energy	$\dot{E}_{sist}$	Wh
Liquid fraction	L_A	–
Thermal efficiency	η_{th}	%
Storage Efficiency	η_{std}	%

3. Validation

3.1. Experimental Setup and Measurements

The proposed model was validated through experimental data reported by El Khadraoui et al. [26]. This work evaluated the performance of an indirect solar dryer (ISD) with and without PCM to study the thermal behavior of the prototype and the effect of heat transfer from the thermal storage system to the air. The proposed ISD and its parts are shown in Figure 2.

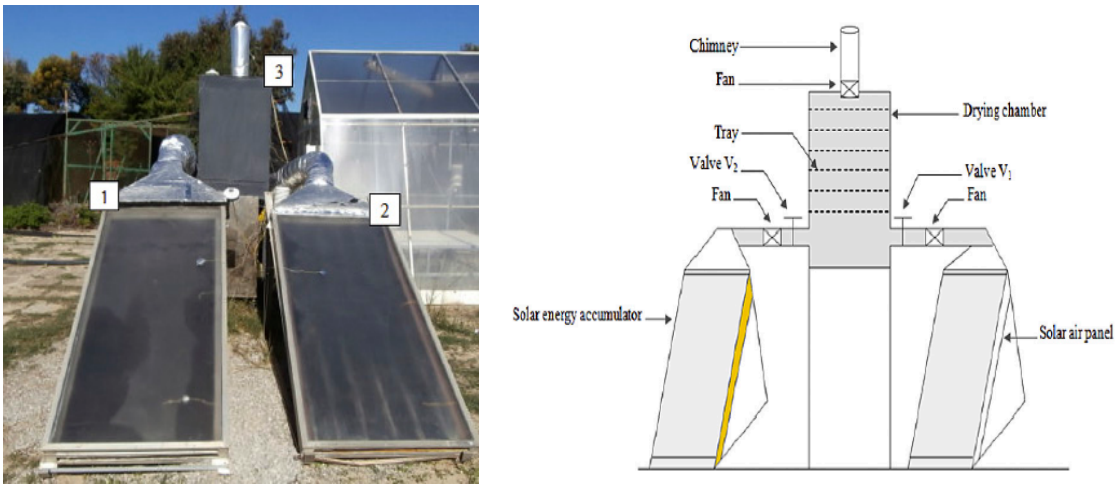

Figure 2. Indirect solar dryer (ISD) prototype, and schematic diagram of the ISD (figure taken from El Khadraoui et al. [26]).

The operation principle of the proposed ISD is shown in Figure 3 and consists of two modes of operation: daytime and nighttime. At daytime (from 6:00 a.m. to 4:00 p.m.), both collectors absorb the incident solar radiation transmitted through the glass cover. The outlet valve of the solar air heater (SAH) without PCM (V1) is open, allowing flow through it while the outlet valve of the SAH with PCM (V2) is closed. At the same time, the PCM receives energy (charging process) by being in contact with the absorber plate. Subsequently, the air from the collector without PCM enters the drying chamber of the ISD. At nighttime (from 4:00 p.m. to 6:00 a.m. of the next day), the outlet valve of the SAH without PCM is closed, and the outlet valve of the SAH with PCM is open (V1 is closed, and V2 is open). Air flows through the collector with PCM while gaining energy from the heat stored by the PCM (discharge process). The stored heat is used at night to continue the drying process.

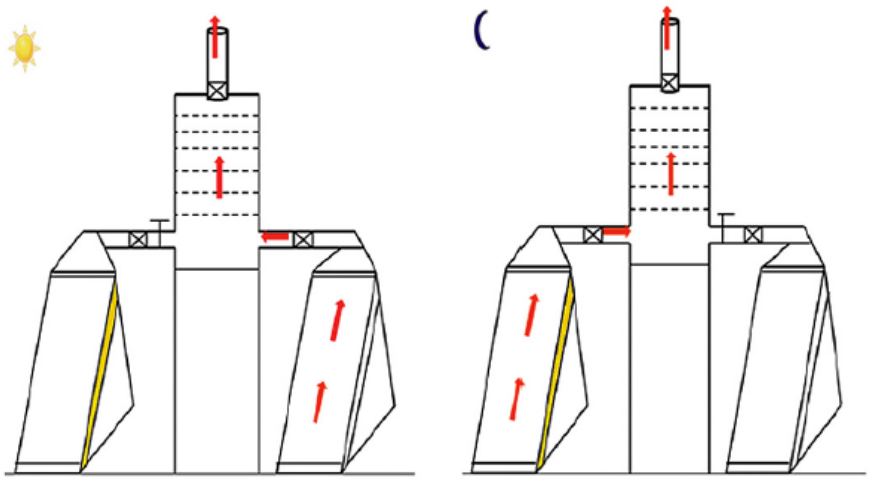

(**a**) (**b**)

Figure 3. Operation principle of the ISD with phase change material (PCM): (**a**) daytime, (**b**) nighttime (figure taken from El Khadraoui et al. [26]).

The prototype was tested in no-load conditions with and without PCM, and the operating conditions are shown in Figure 4.

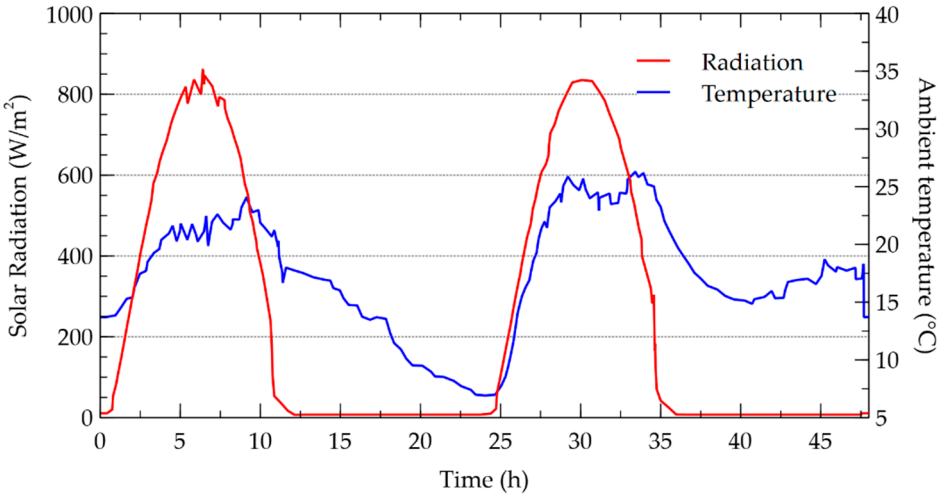

Figure 4. Operation conditions.

3.2. Model Validation

An independent analysis was performed to determine the optimal number of layers to model the PCM. The PCM temperature was simulated with different numbers of PCM layers under the same operating conditions. The results of the independent analysis (Figure 5) show that, after 100 layers, the estimated change in temperature is less than 0.01 °C. A variable time step was selected in the MATLAB/Simulink software program, having a maximum and minimum step of 2.9 and 3.2×10^{-12} s, respectively.

Figure 6 shows the collector air outlet temperature with PCM obtained experimentally by [26], compared with the estimation of the model. According to the results, the thermal model estimates the air outlet temperatures with a mean absolute error (MAE) of 1.24 °C and a root mean square error (RMSE) of 1.34 °C.

This issue is caused by the transition from the collector without PCM to the collector with PCM. At 10 h the air output of the collector without PCM is closed while that of the collector with PCM is open. Since the last collector was operating without air flow all day, it causes a temperature peak when the output valve is opened. The heat absorbed by the collector with PCM calculated by [26] and that estimated by the model are shown in Figure 7. Results show that the model estimates the heat absorbed by the collector with PCM with an MAE of 21.56 W and an RMSE of 30.89 W.

The heat stored by the PCM calculated by [26] and the comparison with that estimated by the model are shown in Figure 8. The model estimates the result with an MAE of 59.73 W and an RMSE of 65.09 W.

The results shown above concerning the estimations given by the thermal model proposed are in agreement with the experimental results reported by [26]. The general validation results obtained are summarized in Table 4.

Table 4. Validation results.

Outlet Variable	MAE	RMSE
Air outlet temperature with PCM	1.24 °C	1.34 °C
Heat absorbed	21.56 W	30.89 W
Heat stored by the PCM	59.73 W	65.09 W

MAE, mean absolute error; RMSE, root mean square error.

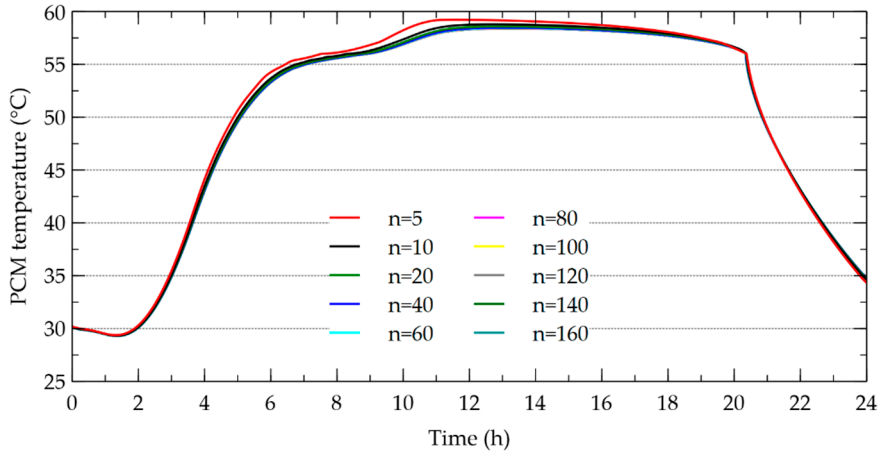

(**a**)

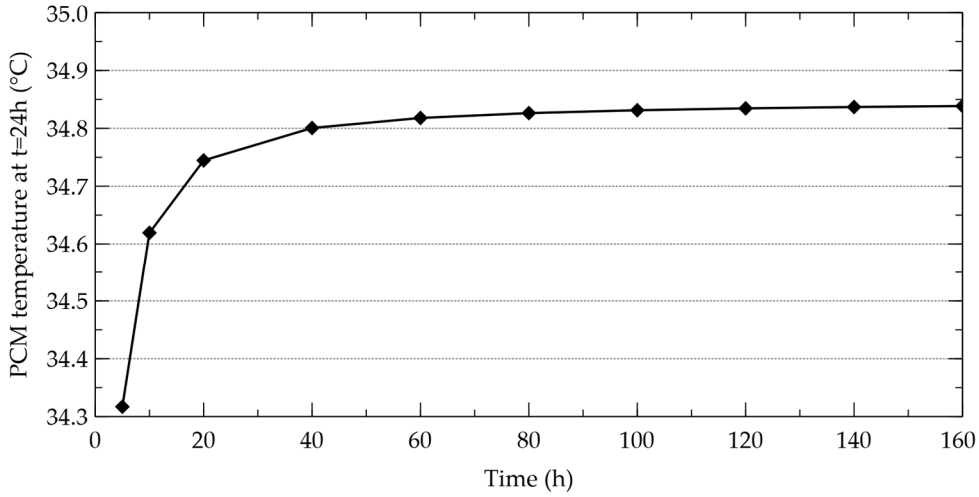

(**b**)

Figure 5. Independent analysis for PCM layers: (**a**) Simulations for different numbers of PCM layers. (**b**) Temperature at 24:00 h for different numbers of PCM layers.

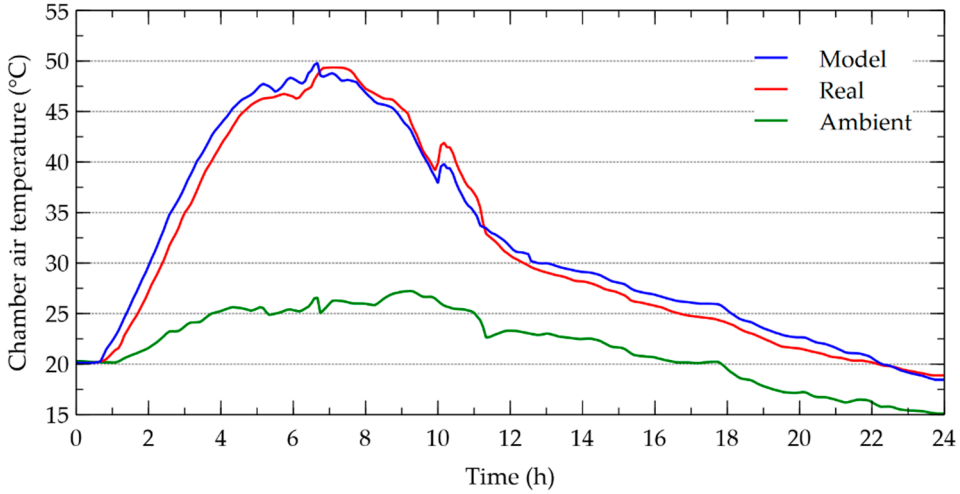

Figure 6. Estimated outlet air temperature with PCM.

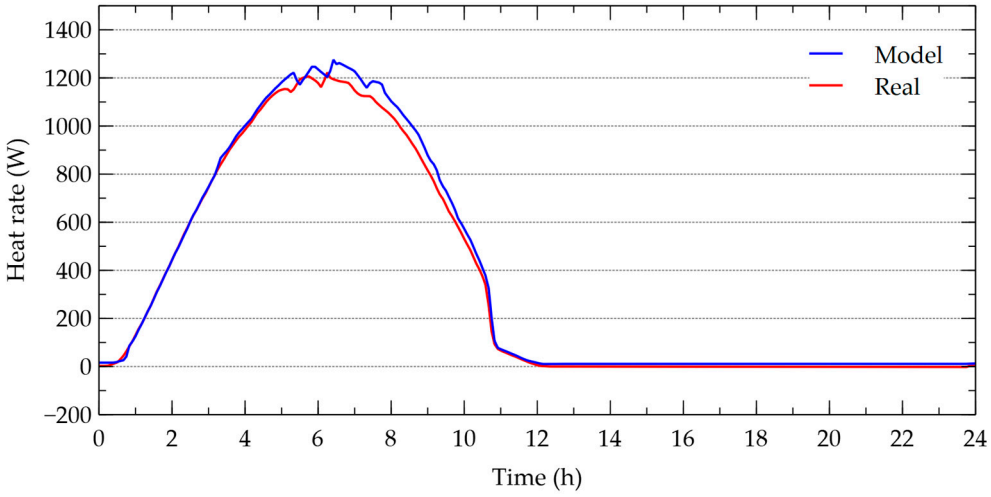

Figure 7. Estimated absorbed heat rate.

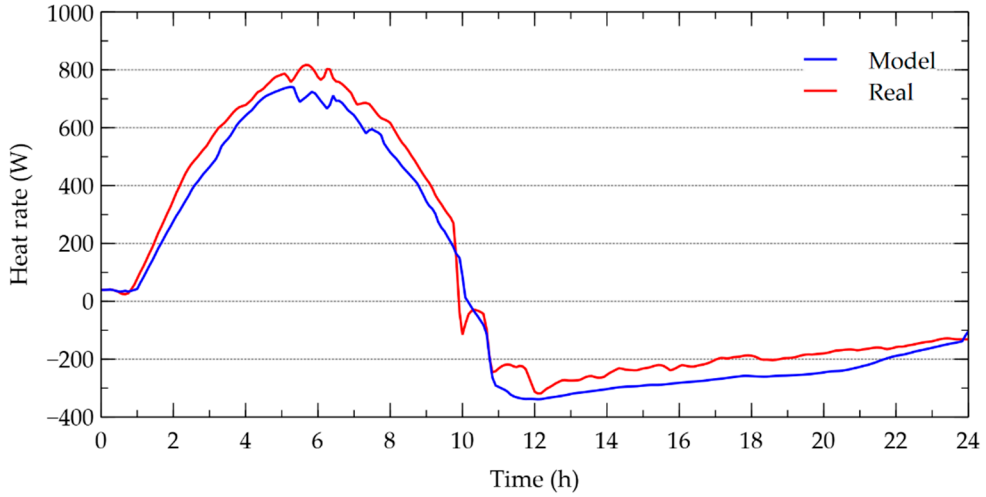

Figure 8. Estimated stored heat rate.

4. Results and Discussions

In this section, the thermal model is used to assess a comparative analysis of the ISD performance considering three different case studies. In case 1, the ISD works alternating with and without PCM collectors under the same operation principle reported by [26]. In case 2, the ISD is operated under continuous airflow and the PCM technology is used throughout 24 h. For case 3, an ISD without PCM and continuous airflow for 24 h is considered in order to establish a comparison base line. All cases were evaluated under the operating conditions presented in Figure 4.

Results of the estimated temperatures of the main components for cases 1, 2, and 3 are shown in Figures 9–11, respectively. As expected, cases 1 and 3 show equal glass cover and absorber plate temperatures during day operation since in both cases the thermal energy is supplied by a collector without PCM. On the other hand, case 2 presents lower temperatures as a result of the thermal energy absorbed by the PCM. As observed experimentally in the validation process, at t = 10 h, case 1 present a discontinuity in temperature estimation caused by the switch from the collector without PCM to the collector with PCM, which was storing energy from the start of the test. However, it can be noted that, during discharge process, case 2 presents similar results as case 1 even though the PCM collector of case 1 was storing energy during the daytime without useful heat delivery.

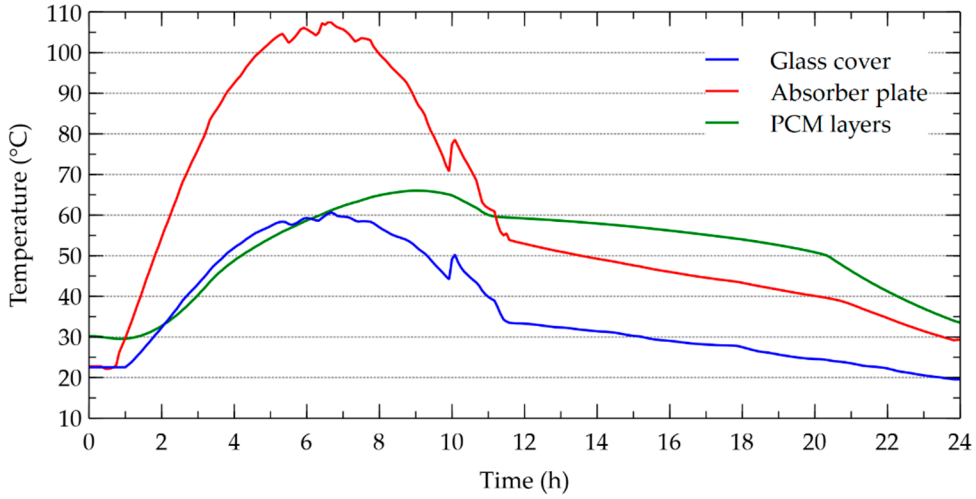

Figure 9. Estimated temperatures of components in case 1.

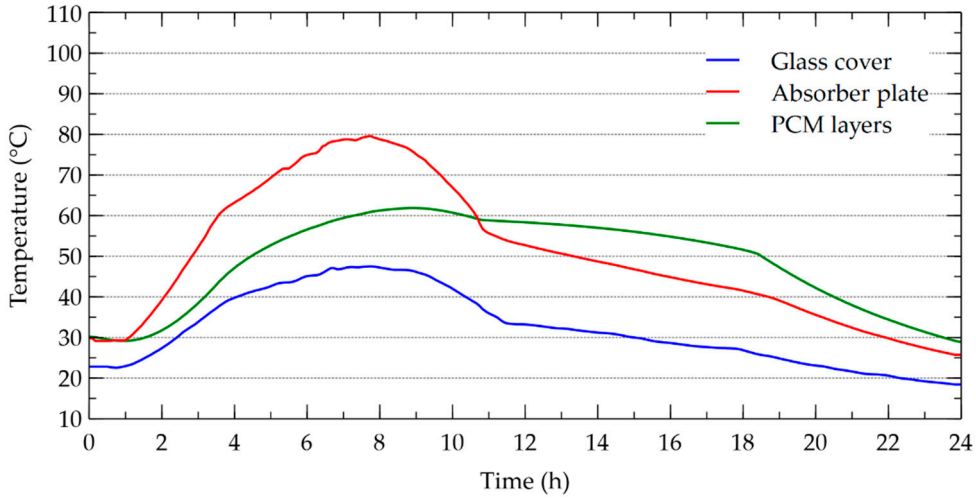

Figure 10. Estimated temperatures of components in case 2.

The useful heat for each of the cases is shown in Figure 12. As obtained for temperatures, the useful heat of case 1 presents the same behavior as that of case 3 during the charge process, and a similar behavior to that of case 2 during the discharge period. The average day and night outlet temperatures are shown in Figure 13 for all cases. Results indicate that the use of PCM in ISD increases the average outlet temperature during the nighttime, thus the operational time of the device is extended. Furthermore, in terms of average outlet temperature, the alternating operation of two solar collectors with and without PCM presents similar discharge results to that shown by using one collector operating with PCM continuously. In fact, the average daytime outlet temperatures are 40.0, 34.1, and 40.1 °C for cases 1, 2, and 3, respectively, and the average nighttime outlet temperatures are 26.0, 25.5, and 20.8 °C for cases 1, 2, and 3, respectively. It can be observed that the difference between cases 1 and 3 for daytime temperature is 0.39 °C. The average daytime temperature of case 2 is lower than that of case 1 with a difference of 5.68 °C, as a result of the simultaneous energy supply to the airflow and accumulation system.

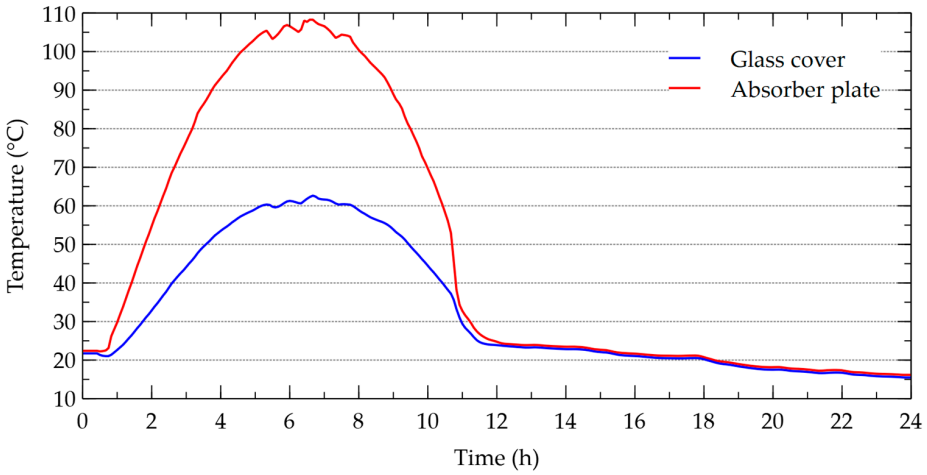

Figure 11. Estimated temperatures of components in case 3.

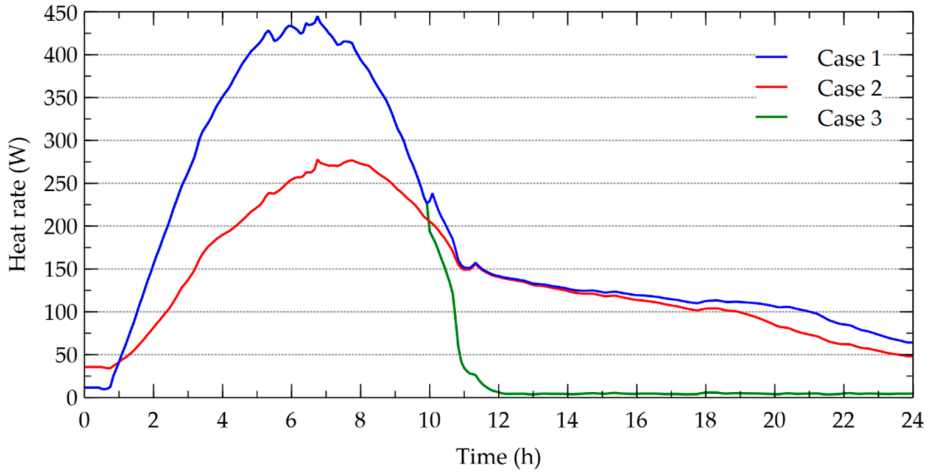

Figure 12. Estimated useful heat rate.

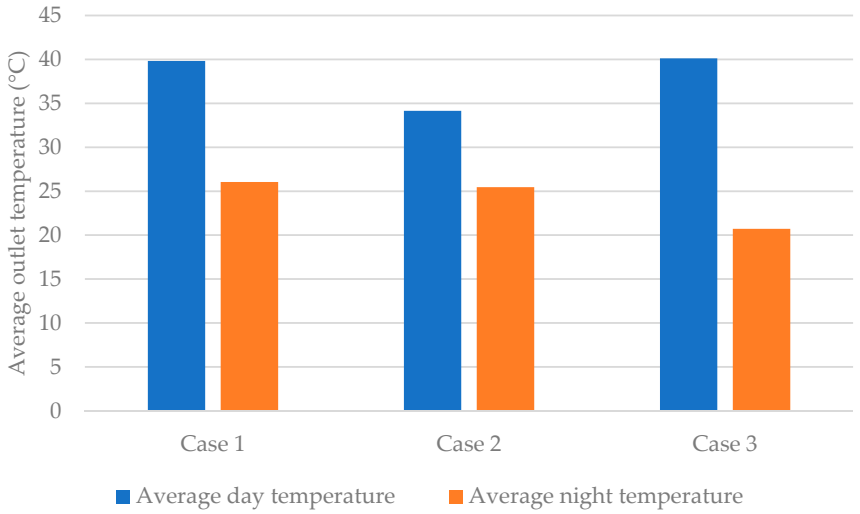

Figure 13. Estimated average outlet temperatures.

Figure 14 shows the total losses considering radiation, convection, and conduction through insulation. Since case 1 uses two collectors exposed to solar radiation, this case presents higher heat losses due to greater area of heat transfer in comparison with those of cases 2 and 3.

The temperature difference between the main components and the surroundings has an important effect in heat losses. In cases 1 and 3, which obtained higher absorber plate temperatures and glass cover temperatures as is showed in Figures 9 and 11, the collectors reach higher heat losses compare to that in case 2 with lower temperatures of its components. Figure 15 shows the PCM stored heat transfer rate for cases 1 and 2. As mentioned above, despite restricting airflow during the charge operation in case 1, the heat rate is not significantly higher than that in case 2. Consequently, cases 1 and 2 are similar in terms of energy storage.

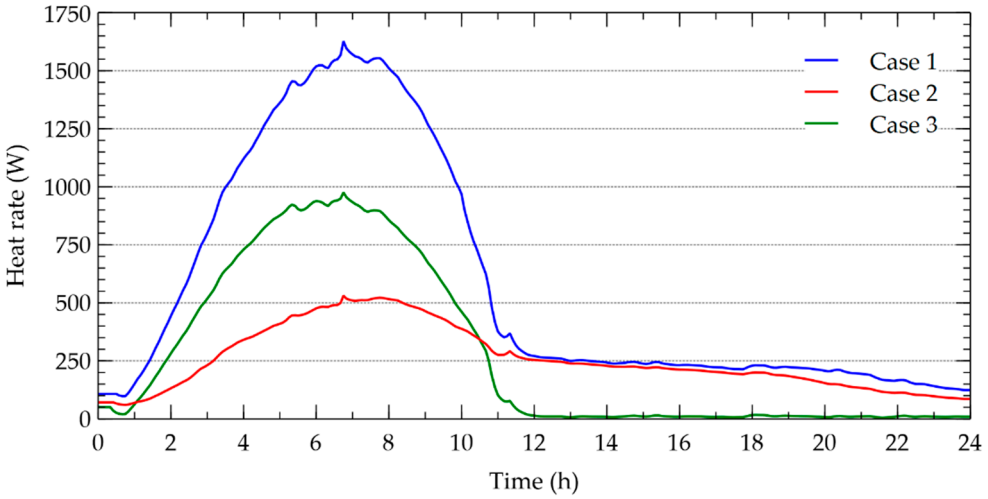

Figure 14. Estimated total losses.

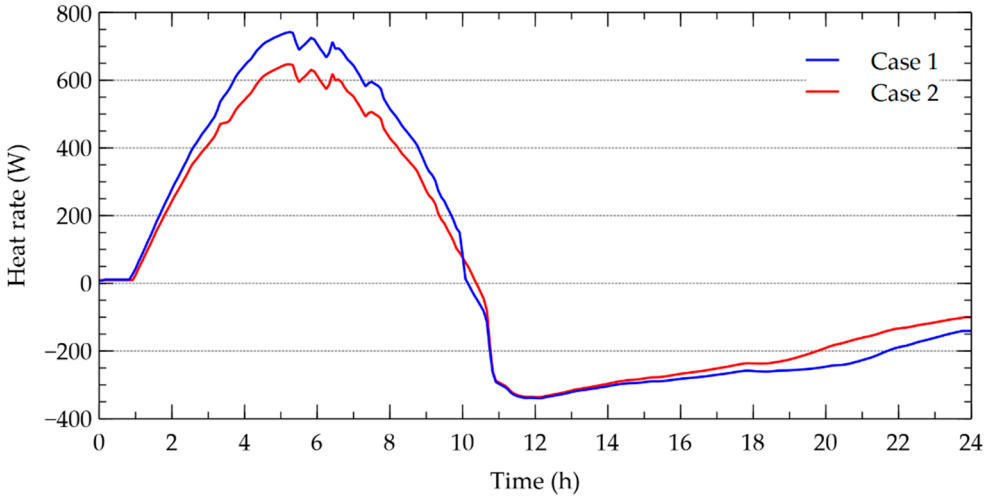

Figure 15. Estimated stored heat rate.

The total accumulated energy in the ISD is shown in Figure 16 for each case. The maximum accumulated energy for cases 1 and 2 is 4.5 and 3.8 kWh, respectively. Cases 1 and 2 (which used PCM) presented higher accumulated energy compared to case 3 (without PCM). This result agrees with the liquid fraction of the PCM presented in Figure 17, where cases 1 and 2 obtain 0.91 and 0.73 of maximum total mass of the PCM in latent heat operation. As shown in Figure 15, the difference between cases 1 and 2 is not as large, considering that PCM collector of case 2 was supplying useful heat and accumulating thermal energy simultaneously, while the collector with PCM in case 1 was operating in an exclusively storing mode during the first ten hours of the test.

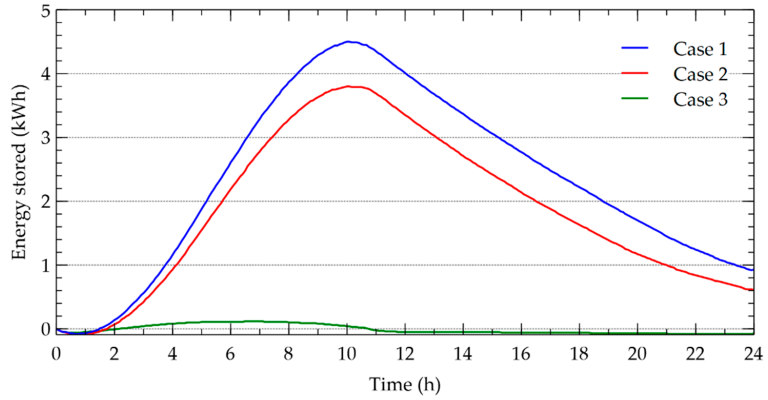

Figure 16. Estimated energy stored by the components.

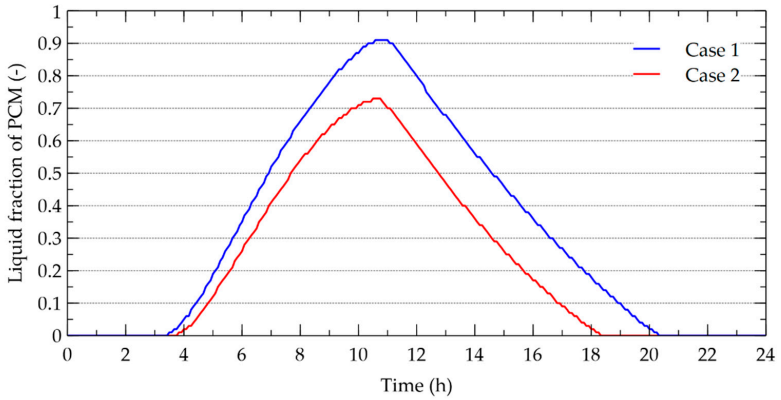

Figure 17. Estimated liquid fraction of PCM.

Thermal efficiency (see Equation (33)) of the ISD and storage efficiency (see Equation (34)) of the PCM are shown in Figure 18. Thermal efficiencies for cases 1, 2, and 3 are 20%, 28%, and 24%, respectively, and the thermal storage efficiencies are 14% and 13% for cases 1 and 2, respectively. Even though part of the energy absorbed in case 2 is being supplied to the air at daytime, the storage efficiency in cases 1 and 2 is similar. The solar collection area in case 1 is double that of the other cases, consequently, the thermal efficiency in case 1 is the lowest of all the cases considered. On the other hand, cases 2 and 3 present higher thermal efficiencies; however, case 2 contributes to solving the solar intermittency issue.

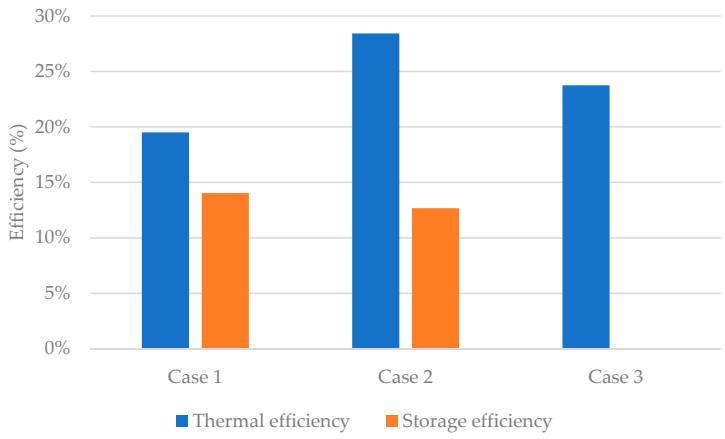

Figure 18. Estimated efficiencies of the ISD.

5. Conclusions

In this article, a thermal reduced model for an ISD with energy storage by PCM was presented. This model was validated using an experimental work from scientific literature. Estimations of the model are in good agreement with the experimental observations, and the performance of the model showed the capability to reproduce the thermal behavior of the device for a variant real condition.

Once the model was validated, the performance of an ISD with and without PCM was analyzed under the operating conditions of the previous work. The thermal model was used to analyze parameters that are difficult to measure experimentally, such as the PCM heat rate, the useful heat, the heat losses, the PCM liquid fraction, and the heat stored by the components. Moreover, three case studies were analytically compared to determine the feasibility of using two alternating collectors with and without PCM, ISD with PCM continuously, or ISD without PCM continuously.

It can be concluded that the use of PCM in ISD contributes to overcoming the issue of intermittent energy, extending the drying operation time, and increasing thermal efficiency from 24% to 28%. On the other hand, restriction of the working fluid of a collector with PCM during charging does not significantly increase discharge performance. Results indicate that there is no important difference between using two alternating collectors with and without PCM compared to the continuous operation of a unique collector with PCM.

Estimated component temperatures, useful heat rate, liquid fraction, and heat stored by the components, present similar behavior in cases 1 and 2 (both with the use of PCM). Nevertheless, the use of two alternating collectors increases the heat transfer area, which causes higher heat losses and lower thermal efficiency of the whole system.

Author Contributions: Conceptualization, C.R., M.P., and M.C.; data curation, C.R., M.P., and M.C.; formal analysis, C.R., M.P., and M.C.; funding acquisition, C.R., M.P., and M.C.; investigation, C.R., M.P., and M.C.; methodology C.R., M.P., and M.C.; resources, C.R., M.P., and M.C.; supervision, C.R., M.P., and M.C.; validation, C.R., M.P., and M.C.; visualization, C.R., M.P., and M.C.; writing—original draft, C.R., M.P., and M.C.; writing—review and editing, C.R., M.P., and M.C. All authors have read and agreed to the published version of the manuscript.

Funding: This research received no external funding.

Conflicts of Interest: The authors declare no conflict of interest.

Nomenclature

A	Area $\left(m^2\right)$
C_p	Specific heat $(J/kg{\cdot}K)$
$\dot{E}$	Energy (W)
g	Gravity $\left(m/s^2\right)$.
h	Heat transfer coefficient $\left(W/m^{2}{\cdot}{}^{\circ}C\right)$
W	Width (m)
H	High (m)
k	Thermal conductivity $(W/m{\cdot}{}^{\circ}C)$
L	Length (m)
m	Mass (kg)
$\dot{m}$	Mass flow (kg/s)
N_u	Nusselt number $(-)$
P_r	Prandalt number $(-)$
$\dot{Q}$	Heat flux (W)
I_c	Solar radiation $\left(W/m^2\right)$
D_H	Hydraulic diameter (m)
Re	Reynolds number $(-)$
t	Time (s)
T	Temperature $({}^{\circ}C)$
V	Velocity (m/s)
v	Kinematic viscosity $\left(m^2/s\right)$

Greek symbols

α	Absorptance $(-)$
β	Volumetric expansion coefficient $(-)$
ε	Emissivity $(-)$
η	Accumulated efficiency $(\%)$
σ	Stefan–Boltzmann constant $\left(W/m{\cdot}K^4\right)$
τ	Transmittance $(-)$

Subscripts

a	Air
amb	Ambient
pa	Absorbed plate
v	Glass cover
conv	Convection
rad	Radiation
co	Collector
std	Storage
U	Useful
out	Outlet
u	Upper
th	Thermal

Acronyms

MAE	Mean absolute error
RMSE	Root mean square error

References

1. Purohit, P.; Kandpal, T.C. Solar crop dryer for saving commercial fuels: A techno-economic evaluation. *Int. J. Ambient. Energy* **2005**, *26*, 3–12. [CrossRef]
2. Kumar, M.; Sansaniwal, S.K.; Khatak, P. Progress in solar dryers for drying various commodities. *Renew. Sustain. Energy Rev.* **2016**, *55*, 346–360. [CrossRef]
3. Karthikeyan, A.; Murugavelh, S. Thin layer drying kinetics and exergy analysis of turmeric (Curcuma longa) in a mixed mode forced convection solar tunnel dryer. *Renew. Energy* **2018**, *128*, 305–312. [CrossRef]
4. Gatea, A.A. Performance evaluation of a mixed-mode solar dryer for evaporating moisture in beans. *J. Agric. Biotechnol. Sustain. Dev.* **2011**, *3*, 65–71.
5. Dhalsamant, K.; Tripathy, P.P.; Shrivastava, S.L. Food and Bioproducts Processing Heat transfer analysis during mixed-mode solar drying of potato cylinders incorporating shrinkage: Numerical simulation and experimental validation. *Food Bioprod. Process.* **2018**, *109*, 107–121. [CrossRef]
6. Oliver, A.; Neila, F.J.; García-Santos, A. Clasificación y selección de materiales de cambio de fase según sus características para su aplicación en sistemas de almacenamiento de energía térmica. *Mater. Construcción* **2012**, *62*, 131–140. [CrossRef]
7. Gil, A.; Medrano, M.; Martorell, I.; Lázaro, A.; Dolado, P.; Zalba, B.; Cabeza, L.F. State of the art on high temperature thermal energy storage for power generation. Part 1—Concepts, materials and modellization. *Renew. Sustain. Energy Rev.* **2010**, *14*, 31–55. [CrossRef]
8. Nkwetta, D.N.; Haghighat, F. Thermal energy storage with phase change material—A state-of-the art review. *Sustain. Cities Soc.* **2014**, *10*, 87–100. [CrossRef]
9. Rodríguez-Cumplido, F.; Gelves, E.P.; Chejne-Jana, F. Recent developments in the synthesis of microencapsulated and nanoencapsulated phase change materials. *J. Energy Storage* **2019**, *24*, 100821. [CrossRef]
10. Arshad, A.; Jabbal, M.; Yan, Y.; Darkwa, J. The micro-/nano-PCMs for thermal energy storage systems: A state of art review. *Int. J. Energy Res.* **2019**, *43*, 5572–5620. [CrossRef]
11. Sharma, A.; Tyagi, V.; Chen, C.; Buddhi, D. Review on thermal energy storage with phase change materials and applications. *Renew. Sustain. Energy Rev.* **2009**, *13*, 318–345. [CrossRef]
12. Haldorai, S.; Gurusamy, S.; Pradhapraj, M. A review on thermal energy storage systems in solar air heaters. *Int. J. Energy Res.* **2019**, *43*, 6061–6077. [CrossRef]
13. Iqbal, K.; Khan, A.; Sun, D.; Ashraf, M.; Rehman, A.; Safdar, F.; Basit, A.; Maqsood, H.S. Phase change materials, their synthesis and application in textiles—A review. *J. Text. Inst.* **2019**, *110*, 625–638. [CrossRef]

14. Reyes, A.; Henríquez-Vargas, L.; Aravena, R.; Sepulveda, F. Experimental analysis, modeling and simulation of a solar energy accumulator with paraffin wax as PCM. *Energy Convers. Manag.* **2015**, *105*, 189–196. [CrossRef]
15. Tchaya, G.B.; Kamta, M.; Havet, M.; Kapseu, C. Thermal performance modelling of solar collector with heat storage. *Int. J. Eng. Syst. Model. Simul.* **2017**, *9*, 53–62. [CrossRef]
16. Atalay, H.; Çoban, M.T.; Kıncay, O. Modeling of the drying process of apple slices: Application with a solar dryer and the thermal energy storage system. *Energy* **2017**, *134*, 382–391. [CrossRef]
17. Vásquez, J.; Reyes, A.E.; Pailahueque, N. Modeling, simulation and experimental validation of a solar dryer for agro-products with thermal energy storage system. *Renew. Energy* **2019**, *139*, 1375–1390. [CrossRef]
18. Hamed, M.; Brahim, A.B. Theoretical Model of a Flat Plate Solar Collector Integrated with Phase Change Material. *J. Electr. Comput. Energy Electron. Commun. Eng.* **2015**, *9*, 1479–1486.
19. Carmona, M.; Gabriel, C.; Humberto, G.; Antonio, B. Reduced Model for a Thermal analysis of a Flat Plate Solar used to estimate the performance for different configurations. In Proceedings of the ASME International Mechanical Engineering Congress and Exposition, Houston, TX, USA, 13–19 November 2015; Volume 57441, pp. 1–12.
20. Dagdougui, H.; Ouammi, A.; Robba, M.; Sacile, R. Thermal analysis and performance optimization of a solar water heater' touan (Morocco) flat plate collector: Application to Te. *Renew. Sustain. Energy Rev.* **2011**, *15*, 630–638. [CrossRef]
21. Carmona, M.; Palacio, M. Thermal modelling of a flat plate solar collector with latent heat storage validated with experimental data in outdoor conditions. *Sol. Energy* **2019**, *177*, 620–633. [CrossRef]
22. Potdukhe, P.; Thombre, S.B. Development of a new type of solar dryer: Its mathematical modelling and experimental evaluation. *Int. J. Energy Res.* **2008**, *32*, 765–782. [CrossRef]
23. Deng, J.; Ma, R.; Yuan, G.; Chang, C.; Yang, X. Dynamic thermal performance prediction model for the flat-plate solar collectors based on the two-node lumped heat capacitance method. *Sol. Energy* **2016**, *135*, 769–779. [CrossRef]
24. Simo-Tagne, M.; Zoulalian, A.; Rémond, R.; Rogaume, Y.; Bonoma, B. Modeling and simulation of an industrial indirect solar dryer for Iroko wood (*Chlorophora excelsa*) in a tropical environment. *Maderas Ciencia Tecnol.* **2017**, *19*, 95–112. [CrossRef]
25. Srinivasan, R.; Balusamy, T.; Sakthivel, M.; Srinivasan, R.; Balusamy, T.; Sakthivel, M. Numerical model of natural convective heat transfer within a solar dryer using an indirect double pass collector Numerical model of natural convective heat transfer within a solar dryer using an indirect double pass collector. *Int. J. Ambient Energy* **2018**, *39*, 830–839. [CrossRef]
26. El Khadraoui, A.; Bouadila, S.; Kooli, S.; Farhat, A.; Guizani, A. Thermal behavior of indirect solar dryer: Nocturnal usage of solar air collector with PCM. *J. Clean. Prod.* **2017**, *148*, 37–48. [CrossRef]
27. Forson, F.; Nazha, M.; Rajakaruna, H. Experimental and simulation studies on a single pass, double duct solar air heater. *Energy Convers. Manag.* **2003**, *44*, 1209–1227. [CrossRef]
28. Bahrehmand, D.; Ameri, M.; Gholampour, M. Energy and exergy analysis of different solar air collector systems with forced convection. *Renew. Energy* **2015**, *83*, 1119–1130. [CrossRef]
29. Bergman, T.L.; Incropera, F.P.; DeWitt, D.P.; Lavine, A.S. *Fundamentals of Heat and Mass Transfer*; John Wiley and Sons: Hoboken, NJ, USA, 2011.